Volkson Press

E-ISSN: 2976-2421
CODEN: JRAOCQ

Journal of Rock Art (JRA)

DOI:http://doi.org/10.65098/jra.01.2026.13.23

RESEARCH ARTICLE

Research on the Weathering Resistance of Phosphate-based Restoration Materials for Helankou Rock Art in Ningxia, China

Shu Jiang[1], Xiaotong Huo[2], Ximo Wang[1], Jinhua Wang[3], Yongkang Cao[1,*]

[1] School of Design, Shanghai Jiao Tong University, Shanghai 200240, China
[2] Shaanxi History Museum, Xi 'an 710061, China
[3] Department of Cultural Heritage and Museology, Fudan University, Shanghai 200433, China
[*] Corresponding Author E-mail: ykcao@sjtu.edu.cn

ARTICLE DETAILS

Article History:

Received 09 Mar 2026
Accepted 20 Mar 2026
Available online 30 May 2026

Online Article Code

ABSTRACT

ABSTRACT

The main diseases of the Helankou rock art are related to delamination, cracking, and spalling caused by the expansion of structural fissures, posing higher demands on the compatibility and weathering stability of the restoration materials. This study investigated a metakaolin-monocalcium phosphate monohydrate (MK-MCPM) phosphate gelling system, formulating both neat paste and aggregate-mixed repair mortars. The materials were subjected to freeze-thaw cycles (20 cycles), wet-dry cycles (20 cycles), and 70°C dry heat aging (300 hours). The mechanical properties, surface hardness, mass loss, and volume stability of the materials were systematically evaluated. The results show that the system exhibits excellent weathering resistance: after freeze-thaw cycles, the material's mass loss rate is consistently below 0.5%, and both strength and surface hardness are stable, with an increasing trend in surface hardness, indicating superior freeze-thaw stability. Wet-dry cycles have minimal impact on compressive strength, but the flexural strength of the aggregate-mixed mortar remains stable and even improves, indicating the effectiveness of the aggregate framework in constraining cracking caused by drying shrinkage. Under more severe dry heat conditions, the mortar system can limit strength loss to less than 10%, with volume changes below 0.6%, showing good high-temperature dimensional and mechanical stability. The study suggests that the MK-MCPM repair mortar has potential for application in the Helankou environment, and the durability evaluation and engineering formulation should focus on tensile performance and interface stability under dry heat conditions, with further improvement in long-term service reliability through aggregate optimization.

KEYWORDS

Restoration Material, Rock Art, Weathering Resistance, Metakaolin, Monocalcium Phosphate Monohydrate

1. INTRODUCTION

The Helankou rock art is located in the canyon area on the eastern side of the Helan Mountain range, Ningxia, China (Figure 1). The substrates primarily consist of Triassic sandstone from the Mesozoic era, mainly composed of stable minerals such as quartz, and the overall rock mass stability is good, with no significant risk of large-scale collapse or sliding (Huo et al., 2024). Preliminary investigations reveal that the structural fissures and unloading fractures that developed before the creation of rock art were mostly large pre-existing fractures, having a limited impact on the overall stability. However, the near-surface sandstone, under long-term differential stress and environmental load coupling, is prone to fissure expansion, leading to damage in the form of parallel, flake-like, or curved destruction, with typical symptoms of hollowing, splitting, and spalling resulting in information loss (Figure 2). Further assessment indicates that crack-driven instability is high, often evolving into irreversible surface sealing, which is the primary target for current conservation efforts (Huo et al., 2025). Therefore, using repair materials compatible with sandstone for reattachment and sealing fissures is a critical and urgent technical path to curb further degradation and reduce ongoing information loss from the rock art.

However, the existing inorganic cementing materials are difficult to meet the restoration requirements of the Helankou rock paintings. Traditional lime mortar has good compatibility but low overall mechanical strength, making it unsuitable for reinforcing high-strength sandstones (Arizzi et al., 2011; Lubelli et al., 2012). Portland cement mortars have higher strength, they risk introducing soluble salts and salt damage, and their physical-chemical compatibility with cultural relic materials is insufficient, so they are no longer preferred for the repair of cultural relics. Modern organic materials, when applied to outdoor stone relics, still face issues such as poor aging resistance, thermal and moisture deformation, and compatibility mismatch with the substrate, limiting their long-term service reliability. In recent years, geopolymer-based repair materials have made progress in stone relic restoration, with phosphate and metakaolin (PMK) powder-water solidification forming an inorganic gelling system that combines high mechanical strength and low soluble salt content, more easily achieving compatibility with inorganic stone materials (Jiang et al., 2025). However,

this system has not been systematically tested for weathering stability and interface durability in the extreme freeze-thaw, wet-dry cycling, and strong sunlight dry-heat coupled environment of Helankou, which is the direct motivation for this study.

From the service environment perspective, freeze-thaw cycles, wet-dry cycling, and dry-heat aging are the three dominant factors determining the adaptability of restoration materials in this region. Rapid warming in spring and rapid cooling in autumn cause surface temperatures to frequently cross 0°C, and winter snowfall further intensifies the "melting-freezing" moisture replenishment and freezing events, creating significant temperature gradients and freezing fronts near the surface of the sandstone. Unfrozen water in the pore medium migrates towards the frozen area under chemical potential and temperature gradients, promoting the growth of segregated ice in the pores and micro-cracks, creating crystallization pressure. When the pressure exceeds the local tensile strength, it induces micro-crack formation and gradual expansion, accelerating cracking and spalling (Deprez et al., 2020; Rempel, 2007). Meanwhile, intermittent rainfall in a strong evaporation environment results in wet-dry cycles, causing capillary pressure fluctuations, dissolution-reprecipitation, and pore structure evolution, weakening particle bonding and causing strength degradation (Deng et al., 2025). Strong sunlight and large diurnal temperature differences also lead to unstable thermal fields and thermal fatigue loads, with solar radiation-induced thermal stresses driving subcritical crack growth, providing conditions for early-stage damage that could lead to spalling. Based on this understanding, the restoration and reinforcement materials studied here aim at two critical applications: reattaching detached pieces and sealing fissures, with weathering evaluation focusing on freeze-thaw resistance, wet-dry cycle resistance, and dry-heat aging. The study emphasizes the strength retention, mass and volume stability, and interface integrity after cyclic actions to support the long-term service reliability of materials in the Helankou rock art environment.

2. MATERIALS AND METHODS

2.1 Materials

In this study, high-activity coal-derived metakaolin (Table 1) was used, purchased from Inner Mongolia Superbrand New Materials Co., Ltd. X-ray fluorescence (XRF) analysis showed that the primary chemical composition of the metakaolin was SiO_2 (51.18 wt%) and Al_2O_3 (45.82 wt%), with low levels of impurity oxides.

2.2 Sample Preparation

All specimens were prepared with a P/Al molar ratio of 0.8. Mortars were formulated with two types of aggregates: mullite (M) and Helankou sandstone (H), each with three different aggregate gradations. Based on the particle size analysis of Helankou sandstone, the aggregate amounts were calculated using the Talbot index (n = 1.0, 1.5, 2.0). The binder-to-sand ratio was consistently 1:1.5. The neat paste was labeled as PMK, while the mortars were labeled as P-M (mullite aggregates) and P-H (Helankou sandstone). Different aggregate gradations were indicated as P-M1.0, P-M1.5, and P-M2.0.

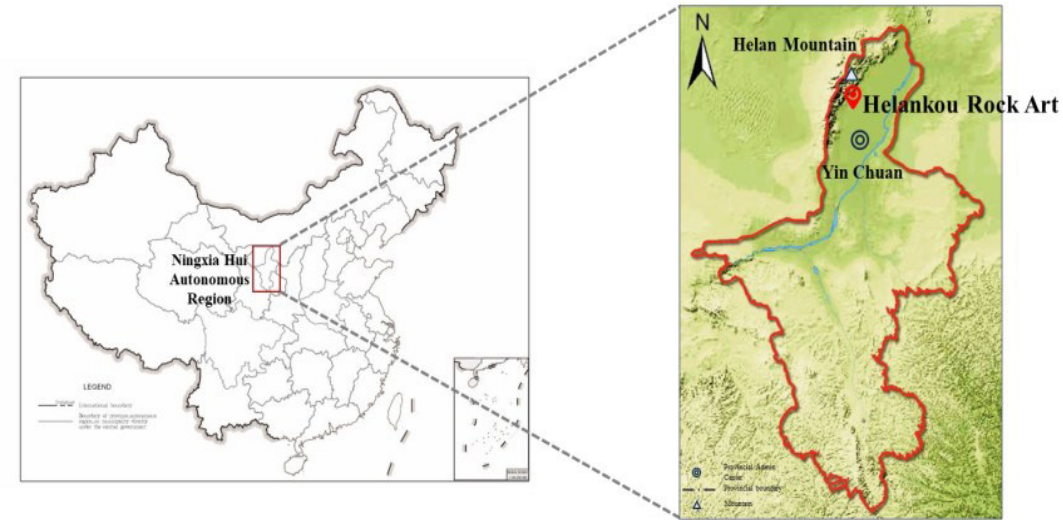

Figure 1 Location of the Helankou Rock Art in Ningxia, China

Figure 2 Typical Diseases in Helankou Rock Art: (a) Splitting with Parts of the Surface already Detached; (b) Hollowing with the Surface Separating from the Rock Body.

Table 1 Chemical Compositions and Producing Area of MK

Sample	Area	SiO_2	Al_2O_3	F_2O_3	K_2O	SO_3	TiO_2	CaO	SUM
MK	Shuozhou	51.18%	45.82%	0.61%	0.16%	0.04%	1.37%	0.26%	99.44%

Monocalcium phosphate monohydrate ($Ca(H_2PO_4)_2·H_2O$, MCPM), ≥92% pure, was purchased from Shanghai Aladdin Biochemical Technology Co., Ltd. Deionized water was used for mixing. Mullite sand was sourced from Henan Bangneng Metal Materials Co., Ltd., and the aggregate selection was based on particle size analysis of Helankou sandstone. The Helankou rock sand was prepared by grinding the rocks from the non-rock-painting area.

The powder materials were weighed precisely and mixed thoroughly before adding the appropriate amount of deionized water. The paste was prepared using an NJ-160S cement paste mixer, with the mixing procedure as follows: low-speed stirring for 60 seconds, a 90-second pause to scrape the surrounding slurry into the pot, followed by high-speed stirring for another 60 seconds. The mortar was prepared using a JJ-5 cement mortar mixer, and aggregate was added during the second 30 seconds of mixing. The prepared paste was poured twice into 160 mm × 40 mm × 40 mm molds, and the specimens were compacted using a ZS-15 cement mortar vibratory table at 12,000 ± 400 rpm. After leveling, the samples were cured at 25°C with 95% relative humidity until they were demolding. After curing, the specimens were tested for weathering resistance.

2.3 Test Methods

2.3.1 Freeze-Thaw Cycling Test

The freeze-thaw cycling test was conducted according to the Standard Test Methods for Basic Performance of Building Mortars (JGJ/T70-2009). Three specimens of each mix were prepared: one as the freeze-thaw specimen (saturated and non-saturated freeze-thaw conditions) and another as a comparison. The freeze-thaw test started after a 28-day curing period. The specimens were taken from the curing box, placed in a 20°C constant-temperature chamber for two days of immersion, with the water level 20 mm above the top of the specimens. After immersion, the specimens were removed, wiped with a damp towel to remove moisture, weighed, and measured for volume. The surface hardness of the specimens was also tested. After these measurements, the specimens were placed in an environmental chamber for freeze-thaw testing. The specimens were frozen for 4 hours at -20°C, then thawed for 4 hours at 20°C (Figure 3). This cycle was repeated 20 times.

2.3.2 Wet-Dry Cycling Test

The specimens, cured for 28 days, were subjected to a wet-dry cycle. The samples were immersed in a constant-temperature water bath at 20°C for 2 hours (Figure 4), then dried in an oven at 70°C for 4 hours for one

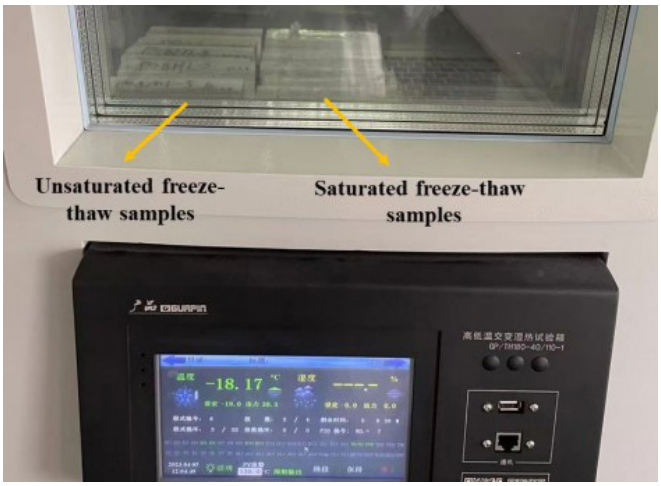

Figure 3 Freeze-thaw Cycling Test Using a Temperature and Humidity Cycling Chamber

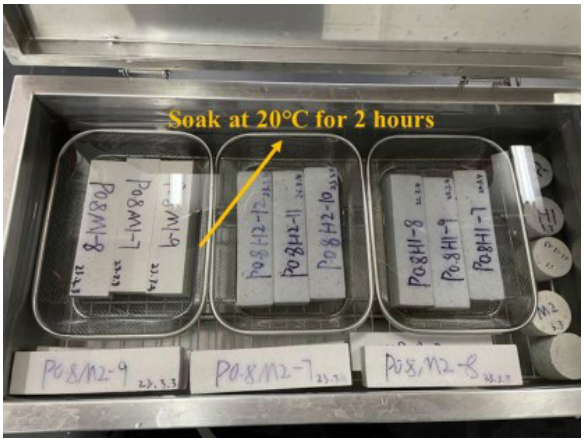

Figure 4 Wet-dry Cycling Test Using a Constant-Temperature Water Bath for Immersion

cycle. This cycle was repeated 20 times. The mass and surface hardness of both the saturated and dry specimens before and after the wet-dry cycles were measured. After the wet-dry cycling tests, the strength of the pre-saturated control specimens was tested, and the strength loss rate and mass loss rate were calculated. The strength loss rates in this experiment include compressive strength loss, flexural strength loss, and hardness loss.

2.3.3 Dry Heat Cycling Test

The specimens were placed in an oven at 70°C for continuous drying for 300 hours (Figure 5). The test aimed to standardize the testing conditions for both experimental and control specimens. After aging, the samples were brought to room temperature, soaked in a 20°C constant-temperature water bath, and tested for mechanical properties. To evaluate the dimensional stability of the specimens under continuous dry heat conditions, the volumes of the specimens after 28 days of curing and after dry heat aging was measured.

2.3.4 Compressive and Flexural Strength Measurements

Compressive and flexural strengths were tested using a WDW-300 electronic universal testing machine according to GB/T 17671–2020 Testing Methods for Cement Mortar Strength (ISO method). After flexural testing, six specimens were used for subsequent compressive strength testing. The flexural strength testing rate was 50 N/s ± 10 N/s, and the compressive strength testing rate was 2.4 kN/s ± 0.2 kN/s (Figure 6).

2.3.5 Surface Hardness Measurement

Surface hardness was measured using a Swiss Proceq Equotip Live Leeb D portable hardness tester. Random measurements were taken on four long edges of the mortar specimens, with 15 measurements per surface. The average value of all four surfaces was used as the surface hardness of each specimen. Each set of specimens consisted of three test samples, and the average value of the three specimens was recorded as the surface hardness value.

2.3.6 Volume Change Measurement

After demolding, the length of each specimen's fixed long edge was measured at multiple stages using a vernier caliper, with five measurements taken per specimen. The average of these readings was used to calculate the volume change rate.

3. RESULTS AND DISCUSSION

3.1 Freeze-Thaw Performance

3.1.1 Compressive and Flexural Strength

After 20 freeze-thaw cycles, the compressive and flexural strengths of the specimens remained stable, showing no signs of continuous deterioration. The neat paste (PMK) exhibited a compressive strength increase from 36.8 MPa to 39.2 MPa under saturated freeze-thaw conditions, with a loss rate of −6.5% (Figure 7). In non-saturated conditions, the compressive strength remained at 37.4 MPa, with a loss rate of −1.6%. The flexural strength increased from 4.3 MPa to 4.4 MPa under saturated conditions (−2.3% loss), while in non-saturated conditions, it dropped slightly from 4.3 MPa to 4.2 MPa (+2.3% loss; Figure 8). These results indicate that the system's mechanical response under freeze-thaw conditions is controlled by the water content.

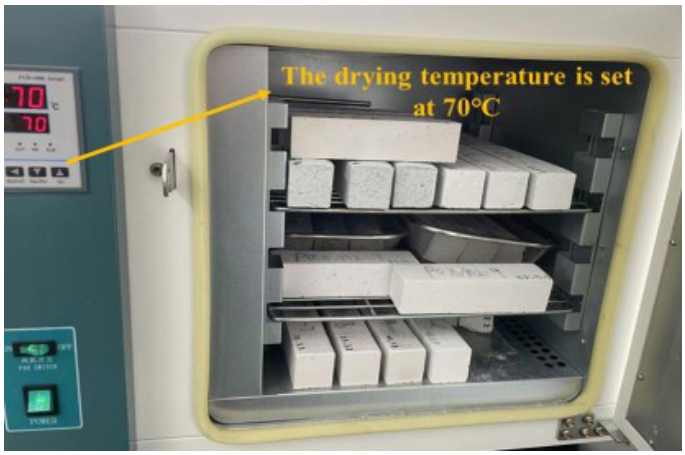

Figure 5 Dry Heat Cycling Test Using an Oven for Drying

Figure 6 Flexural and Compressive Strength Measurements Conducted with a WDW-300 Electronic Universal Testing Machine: (a) Flexural Strength Test; (b) Compressive Strength Test.

Saturated cycles tend to show strength retention or improvement, while non-saturated conditions result in more significant reductions in flexural strength.

For the mortars with added aggregates, the strength and loss rate responses varied significantly. The P-M (mullite) mortar had a compressive strength range of 43.6–51.7 MPa before freeze-thaw cycling. After 20 cycles, the compressive strength ranged from 42.6–52.2 MPa under saturated conditions and 42.9–50.7 MPa under non-saturated conditions. The compressive loss rates ranged from −1.0% to +2.3% in saturated conditions and from +1.6% to +4.7% in non-saturated conditions. The flexural strength of P-M ranged from 5.3–6.0 MPa, increasing to 5.8–6.6 MPa under saturated conditions (−3.6% to −13.2% loss) and 5.2–5.8 MPa under non-saturated conditions (0–+7.1% loss). This indicates that in the absence of sufficient water, slight reductions in tensile properties may occur.

In comparison, the P-H (Helankou sandstone) mortar exhibited lower strength levels, with compressive strength ranging from 10.3–13.2 MPa before freeze-thaw cycling and flexural strength from 2.1–2.8 MPa. After the freeze-thaw cycles, the compressive strength showed negative losses in both saturated and non-saturated conditions (around −1.0% to −4.5%), while flexural strength mostly exhibited positive losses (saturated conditions: +3.8% to +7.1%; non-saturated conditions: 0–+10.7%). This suggests that the freeze-thaw response of the P-H system is more pronounced in terms of interface-related degradation in flexural strength.

Regarding the effect of aggregate gradation, P-M1.5 demonstrated both high strength and low variation in loss rates, while P-M1.0 showed greater sensitivity under non-saturated conditions. For P-H, the 1.0 gradation had higher strength but higher flexural loss, while the 2.0 gradation exhibited lower strength but lower losses, reflecting the trade-off between strength levels and freeze-thaw retention.

These observations can be explained through the pore pressure-interface channel mechanism for freeze-thaw damage. Freeze-thaw damage in concrete or gelling materials typically arises from the hydraulic or osmotic pressure generated by the volume expansion of freezing pore water. Micro-cracks tend to initiate and propagate in pore-rich areas and the interfacial transition zone (ITZ), which makes flexural strength more sensitive than compressive strength. Under saturated freeze-thaw conditions, PMK and P-M generally exhibit negative loss rates, suggesting that continued reactions and product deposition/pore refinement still occur, leading to a densification effect that counters freeze-thaw expansion (Powers, 1975; Chen et al., 2024). Similar phenomena of high strength retention or improvement have been reported in phosphate-based gelling materials, further supporting the results of this study (Yang et al., 2022; Feng et al., 2024).

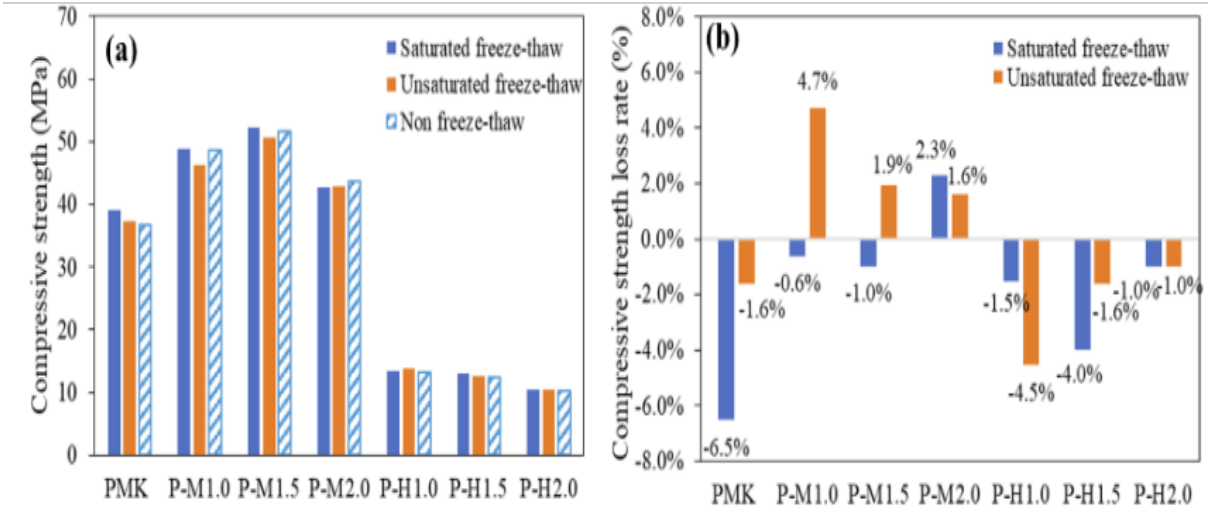

Figure 7 Comparison of Compressive Strength under Two Freeze-thaw Conditions after 28 Days: (a) Compressive Strength; (b) Compressive Strength Loss Rate.

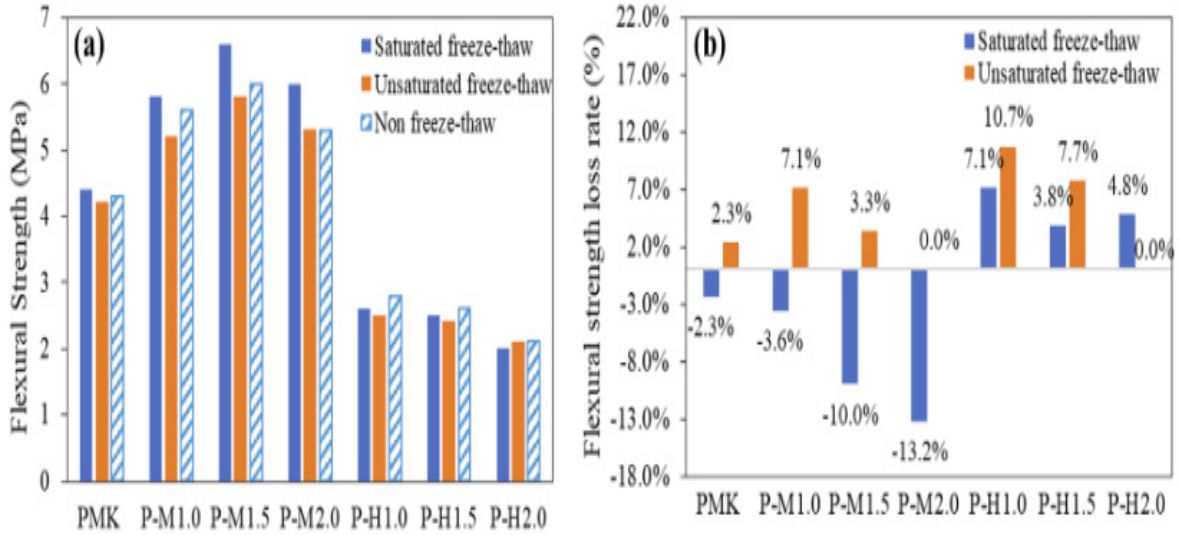

Figure 8 Comparison of Flexural Strength under Two Freeze-thaw Conditions after 28 Days: (a) Flexural Strength; (b) Flexural Strength Loss Rate.

3.1.2 Surface Hardness

Under saturated conditions, after 20 freeze-thaw cycles, the surface hardness of all specimens did not decrease; in fact, it generally increased (Figure 9), indicating that the system demonstrated good surface stability under freeze-thaw and wet conditions. The surface hardness of the neat paste (PMK) increased from 515 HLD to 545 HLD, with a change rate of −5.8%. The P-M system (mullite aggregates) showed a relatively high surface hardness before freeze-thaw cycling (421–489 HLD). After cycling, the surface hardness ranged from 457 to 490 HLD, with changes between −0.2% and −8.6%. The P-H system (Helankou sandstone aggregate) had a lower initial hardness (278–282 HLD), which increased to 328–364 HLD after cycling, with a change rate of −18.0% to −29.1%. Therefore, in terms of absolute values, the surface hardness ranking was PMK ≈ P-M > P-H. In terms of relative changes, the order was P-H > PMK > P-M, with P-H showing the largest improvement, though its surface hardness remained lower than that of P-M.

The observed increase in surface hardness and the negative loss rate suggest that the freeze-thaw phase was not dominated by surface erosion or softening, but rather by surface densification caused by ongoing reactions and pore refinement. Comparing the materials, P-M exhibited higher surface hardness before freeze-thaw cycling, with smaller variations, indicating a more stable surface and interface structure. In contrast, P-H had lower initial hardness but showed a larger increase, suggesting that the near-surface layer had more pores and defects that could be "repaired or filled" through hydration or deposition. However, due to limitations imposed by the aggregate and ITZ quality, its final surface hardness remained lower than P-M.

Further analysis of the gradation effect revealed that for P-M, gradations of 1.0/1.5 resulted in mild increases in hardness (−0.2% and −1.9%), while the 2.0 gradation showed a more noticeable increase (−8.6%). For P-H, the largest improvement occurred in the 1.0 gradation (−29.1%), indicating a strong surface densification effect. However, this advantage did not translate into higher absolute hardness, further reinforcing that the controlling factors for P-H were more related to the interface and aggregate properties.

3.1.3 Mass Loss Rate

The mass loss rate provides a direct indication of the extent of surface spalling and particle detachment after freeze-thaw cycling. According to the GB/T 50082 criteria for quick freeze testing, when the mass loss rate reaches 5% (often accompanied by a compressive strength loss rate of 25%), the test is typically stopped, and the durability is evaluated.

In this study, after 20 freeze-thaw cycles under saturated conditions, the mass loss rates were very low (Figure 10). The mass loss rate for PMK was 0.1%, while for P-M1.0/1.5/2.0, it was 0.0%. For P-H1.0, P-H1.5, and P-H2.0, the mass loss rates were 1.4%, 2.7%, and 3.4%, respectively. All values were significantly lower than the 5% threshold, indicating that no significant surface erosion or exposure of aggregates occurred during freeze-thaw cycling. The specimens maintained good macro-structural stability. Furthermore, the compressive strength loss rates were well below 25%, providing consistent evidence that the material retained both mechanical properties and surface integrity under freeze-thaw conditions. This demonstrates the high freeze-thaw resistance of the materials.

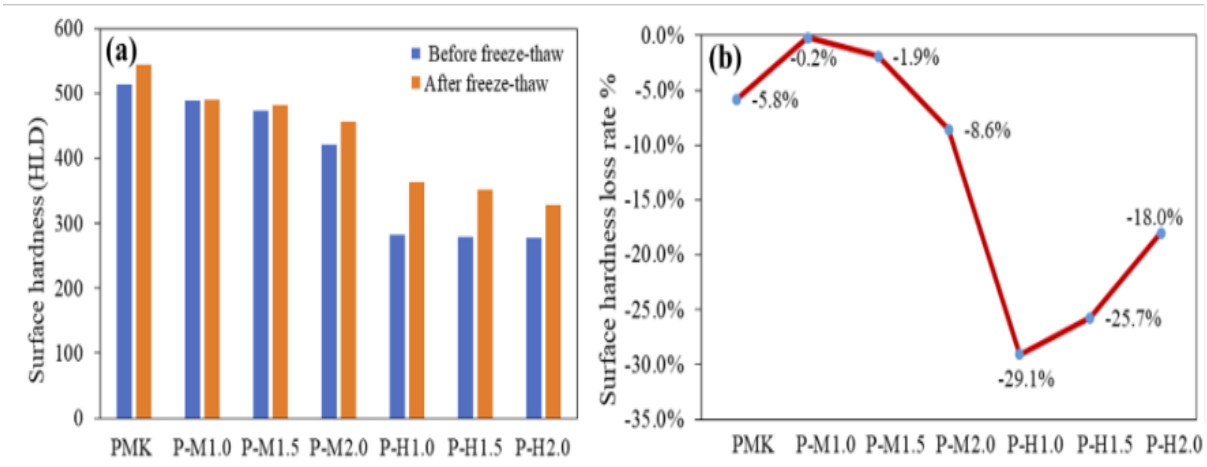

Figure 9 (a) Surface Hardness before and after Freeze-thaw Cycling; (b) Surface Hardness Loss Rate.

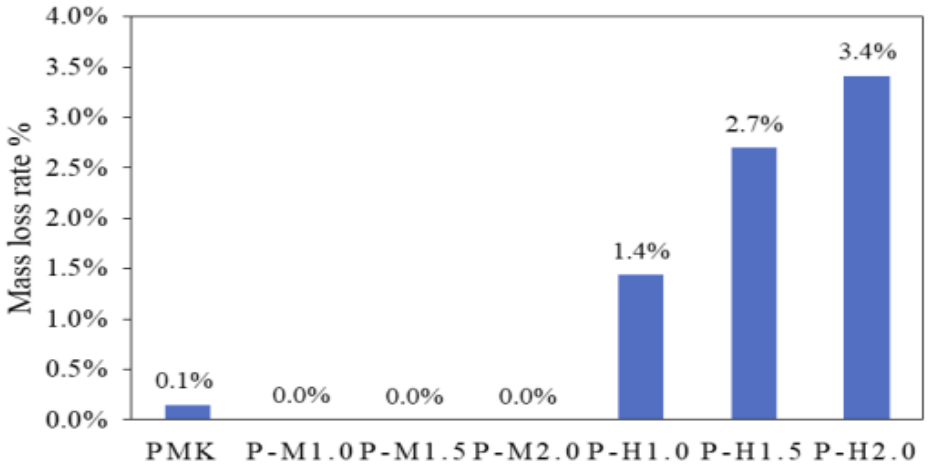

Figure 10 Mass Loss Rate after Freeze-thaw Cycling

3.2 Wet-Dry Cycling Performance

3.2.1 Compressive and Flexural Strength

After wet-dry cycling, all systems showed varying degrees of improvement in compressive strength (Figure 11), indicating that the wetting phase of the cycle promoted continued reactions and pore filling, positively contributing to the compressive load capacity. The compressive strength of PMK increased from 36.8 MPa to 38.7 MPa, with a loss rate of −5.16%. The P-M mortar with mullite aggregates showed an increase in compressive strength from 43.6–51.7 MPa to 46.5–54.4 MPa, with a loss rate ranging from −1.16% to −11.93%, with P-M1.0 showing the largest improvement. The P-H mortar with Helankou sandstone aggregate showed an increase from 10.3–13.2 MPa to 10.4–19.4 MPa, with a loss rate ranging from −0.97% to −46.97%, with the most significant improvements in the P-H1.0 and P-H1.5 gradations. Overall, the inclusion of aggregates significantly raised the baseline compressive strength (P-M ≫ PMK > P-H), and the materials retained or further improved their strength after the wet-dry cycling, reflecting the excellent volume stability and structural recoverability of the systems.

In contrast to compressive strength, flexural strength was more sensitive to wet-dry cycling, showing a clear contrast between the neat paste and the mortars (Figure 12). The flexural strength of PMK dropped sharply from 4.3 MPa to 0.8 MPa (a loss of +81.40%), showing that dehydration shrinkage during the drying phase more easily induced microcracks in the paste, weakening its tensile load capacity. In contrast, the mortars with aggregates did not experience such a significant decline in flexural strength. The flexural strength of P-M increased from 5.3–6.0 MPa to 6.4–6.7 MPa (a loss rate of −11.67% to −20.75%), while P-H flexural strength increased from 2.1–2.8 MPa to 2.1–3.1 MPa (a loss rate of 0% to −15.38%). These results indicate that the aggregate framework effectively restrained the drying shrinkage and microcrack propagation, maintaining the tensile strength of the mortar during the wet-dry cycles. This also highlights that for this type of phosphate-based restoration material, the major durability limitation under wet-dry cycling lies in the tensile properties of the neat paste, while the introduction of aggregates improves its overall durability.

The drying phase of the wet-dry cycle induces moisture gradients and shrinkage strain at the matrix and interface, which can lead to microcracks in the matrix or near the ITZ. This phenomenon, frequently observed in studies of concrete and mortar under wet-dry cycling, primarily damages the tensile properties, such as flexural strength (Song et al., 2021; Dehestani et al., 2020). Meanwhile, the aggregates significantly constrain the matrix's shrinkage, reducing local strain concentration and slowing crack development. This constraint effect is particularly beneficial in maintaining the flexural strength of mortars compared to the neat paste (Hong et al., 2023; Maruyama et al., 2018). Furthermore, the wet phase of the wet-dry cycle can promote the continued reaction and deposition of unreacted components, mitigating the drying damage and potentially allowing compressive strength to either maintain or improve. This "cyclic wetting promoting mid-term strength recovery" phenomenon has been reported in studies of related materials under wet-dry cycling conditions (Hu et al., 2024; Bui et al., 2022).

3.2.2 Surface Hardness

The surface hardness measurements after wet-dry cycling are shown

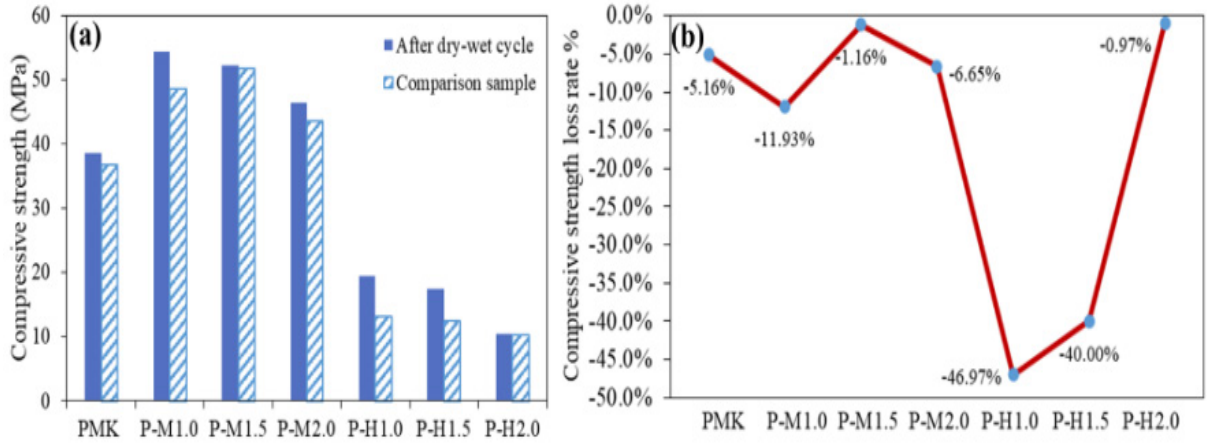

Figure 11 (a) Comparison of Compressive Strength between Specimens after Wet-dry Cycling and Control Specimens; (b) Compressive Strength Loss Rates.

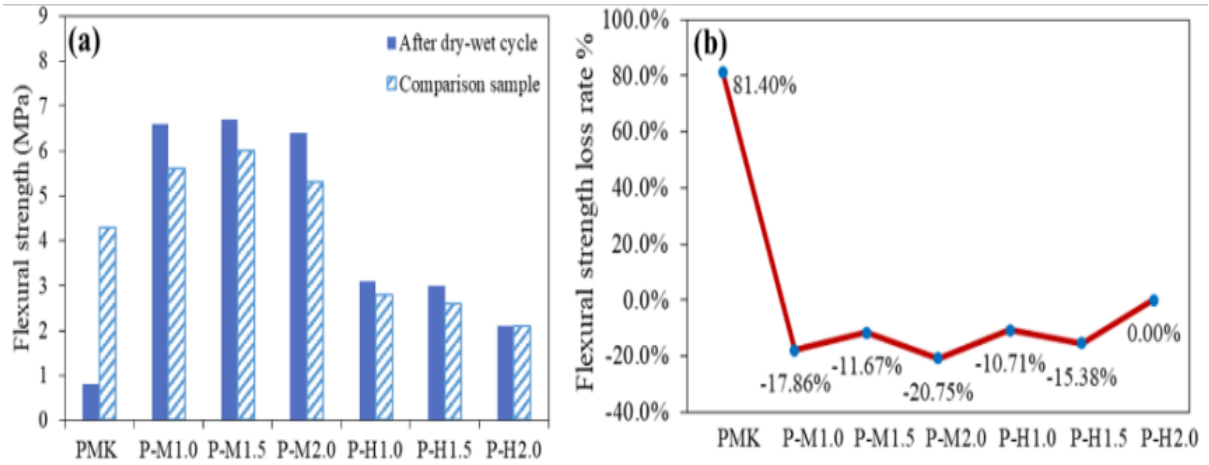

Figure 12 (a) Comparison of Flexural Strength between Specimens after Wet-dry Cycling and Control Specimens; (b) Flexural Strength Loss Rates.

in Figure 13. After completing the wet-dry cycling, the surface hardness of the neat paste (PMK) decreased from 491 HLD to 477 HLD, with a loss rate of 2.85%, indicating that the drying phase of the cycle induced shrinkage and microcrack accumulation on the surface, which reduced the rebound response.

For the mortars with aggregates, the changes in surface hardness were also observed, with the degree of loss closely linked to the type of aggregate and its gradation. The mullite mortar (P-M) showed a decrease in hardness from 496–531 HLD to 473–483 HLD, with a loss rate ranging from 4.6% to 9.0%. The greatest reduction was observed in P-M1.0 (531 → 483 HLD, 9.0%), while P-M1.5 and P-M2.0 exhibited more stable hardness values. The P-H mortar (Helankou sandstone aggregate) showed a decrease in hardness from 391–418 HLD to 327–366 HLD, with a loss rate of 12.4%–16.4%, which was significantly higher than the P-M system, and the degradation became more pronounced with increasing gradation (P-H2.0 had the largest reduction, 391 → 327 HLD, 16.4%).

Overall, the results indicate that the surface hardness loss after wet-dry cycling followed the order: P-H > P-M > PMK. While the P-M system showed better stability in maintaining surface hardness, the P-H system exhibited a more significant decrease, reflecting its greater sensitivity to drying shrinkage and interface damage. The introduction of aggregates, especially mullite, effectively improved the resilience of the material under these cycling conditions.

3.2.3 Mass Loss Rate

The mass loss rate, evaluated in the saturated state, reflects the extent of surface spalling and particle detachment due to wet-dry cycling. As shown in Figure 14, the mass loss rates after wet-dry cycling were all very low across the different specimens, ranging from 0.04% to 0.47%, indicating minimal surface erosion or material loss. The neat paste (PMK) showed a mass loss rate of 0.47%, which was higher than that of the two types of mortars, with P-M and P-H showing values between 0.05%–0.10% for P-M and 0.04%–0.08% for P-H. These results demonstrate that the introduction of aggregates effectively suppressed the macroscopic degradation of mass caused by the wet-dry cycles, likely due to the constraint of shrinkage deformations and the prevention, which affects its tensile properties.

The differences between the two types of mortars were minimal, with both remaining well below the 5% threshold commonly used in durability evaluations. This suggests that, under wet-dry cycling conditions, the materials maintained good dimensional stability and surface integrity. The results also indicate that the main degradation mechanism for this system under wet-dry cycling conditions is the accumulation of microcracks that impact mechanical properties, especially flexural strength and surface hardness, rather than macro-level mass loss due to surface peeling.

3.3 Dry-Heat Cycling Performance

3.3.1 Compressive and Flexural Strength

The results from the dry-heat aging process are shown in Figures 15 and 16, demonstrating significant irreversible structural changes. The neat paste (PMK) showed a marked decrease in strength under dry-heat

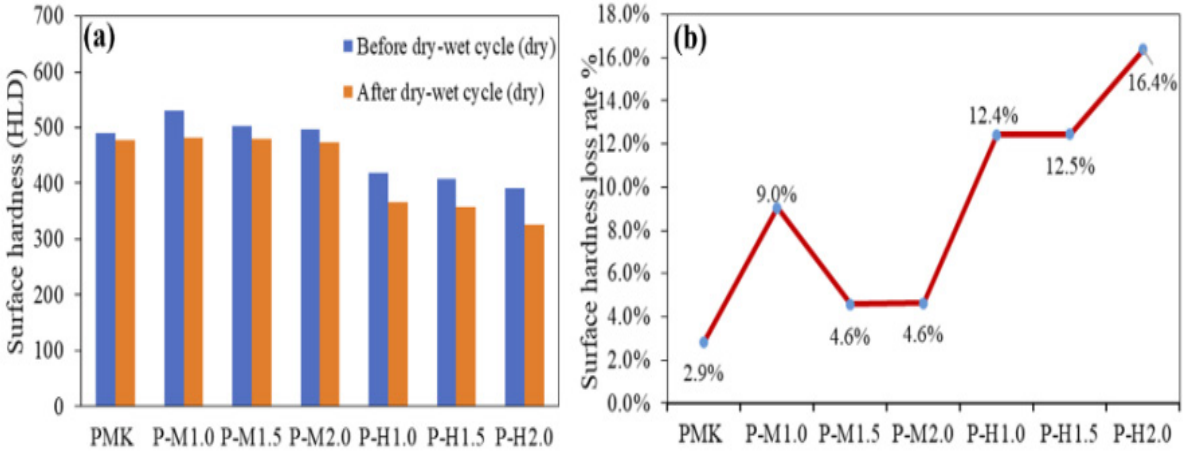

Figure 13 (a) Surface Hardness of Dry Specimens before and after Wet-dry Cycling; (b) Surface Hardness Loss Rate.

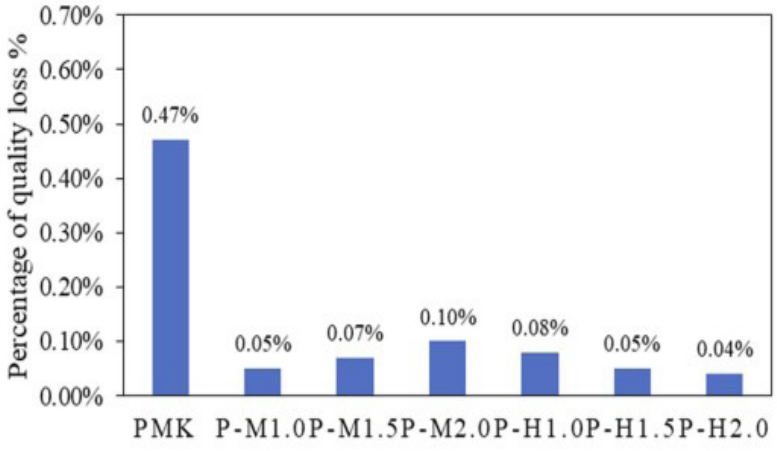

Figure 14 Mass Loss Rate of Specimens before and after Wet-dry Cycling

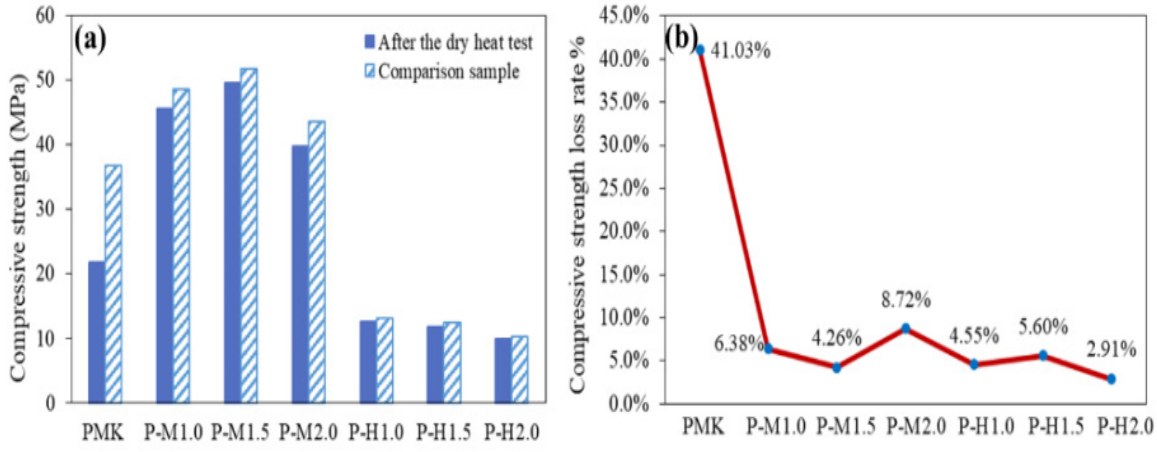

Figure 15 (a) Compressive Strength Comparison between Dry-heat Specimens and Control Specimens; (b) Compressive Strength Loss Rate.

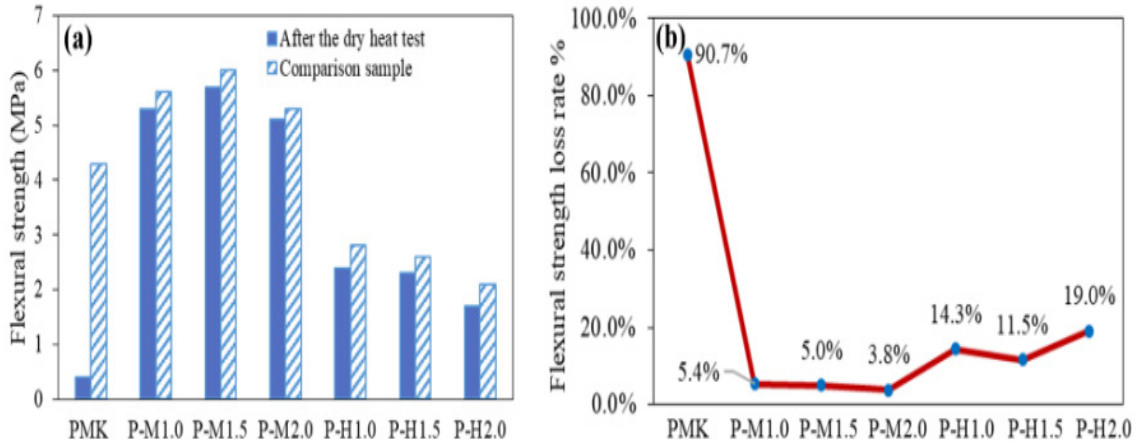

Figure 16 (a) Flexural Strength Comparison between Dry-heat Specimens and Control Specimens; (b) Flexural Strength Loss Rate.

aging. The compressive strength dropped from 36.8 MPa to 21.7 MPa (a loss rate of 41.03%), and the flexural strength decreased sharply from 4.3 MPa to 0.4 MPa (a loss rate of 90.70%), indicating that the neat paste was particularly susceptible to deterioration in tensile capacity under dry-heat conditions.

In contrast, the mortars with aggregates showed significantly improved strength retention. For the P-M mortar, the compressive strength loss was only between 4.26%–8.72%, and the flexural strength loss ranged from 3.77% to 5.36%, demonstrating the most stable dry-heat durability. The P-H mortar exhibited a compressive strength loss between 2.91%–5.60%, while the flexural strength loss ranged from 11.54% to 19.05%. The P-H2.0 gradation was the most sensitive, suggesting that the sandstone-based system was still more prone to interface defects and crack propagation, affecting its tensile properties.

Overall, the key risk under dry-heat aging is the brittle degradation of the tensile properties in the neat paste. However, the introduction of aggregates, especially mullite aggregates, significantly alleviates this issue, providing better protection against dry-heat aging.

The strength degradation caused by dry-heat aging is primarily driven by two heat-moisture coupling processes. First, continuous drying at 70°C induces moisture migration and shrinkage strain, promoting the formation and expansion of microcracks at the surface and in the interface defect zones, making the flexural strength particularly sensitive to the effects of aging. The aggregate's constraint effect reduces shrinkage and crack propagation, which helps maintain flexural strength (Bisschop & van Mier, 2002). Second, phosphate-based gelling phases may undergo dehydration or phase transitions under elevated temperatures, leading to solid-phase volume shrinkage and structural relaxation, weakening the material's load-bearing capacity. Similar findings have been reported in studies on magnesium-potassium phosphate systems, where increased temperatures cause the primary hydration products (e.g., K-struvite) to dehydrate and decompose, resulting in strength reduction. Thermal stability issues become more pronounced when the temperature exceeds or approaches 70°C (Xu et al., 2021; Yuanquan et al., 2023).

3.3.2 Surface Hardness

After dry-heat aging, the surface hardness of all systems decreased (Figure 17), indicating that prolonged exposure to high temperatures and dehydration weakened the near-surface structure. The neat paste (PMK) decreased from 516 to 482 HLD, with a loss rate of 6.6%. The P-M system (mullite aggregates) had a higher initial hardness range (506–535 HLD), which decreased to 475–492 HLD after aging, with a loss rate between 6.1%–8.0%, showing relatively small fluctuations. The P-H system (Helankou sandstone aggregate) had a lower initial hardness (392–410 HLD), which dropped to 343–376 HLD after aging, with a loss rate ranging from 4.1% to 16.3%, showing significantly higher variability. The largest decrease was observed in the P-H2.0 gradation (16.3%).

Overall, the absolute surface hardness after dry-heat aging followed the trend: P-M ≈ PMK > P-H, though the P-H system was more sensitive to gradation and interface conditions. This result is consistent with moisture migration, shrinkage microcrack accumulation, and the potential dehydration and relaxation processes of the phosphate gelling phase under dry-heat conditions, further supporting the

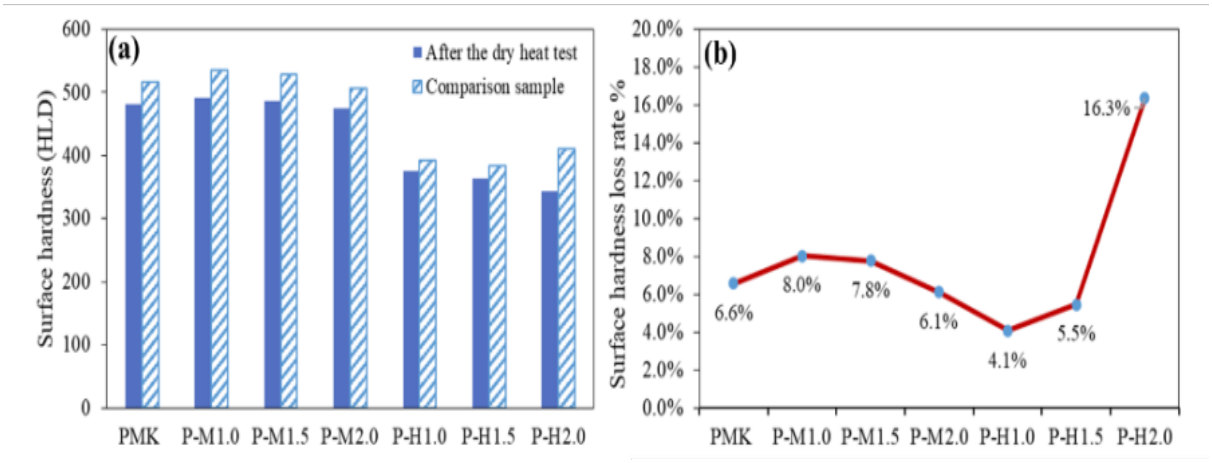

Figure 17 (a) Surface Hardness Comparison between Dry-heat Specimens and Control Specimens; (b) Surface Hardness Loss Rate.

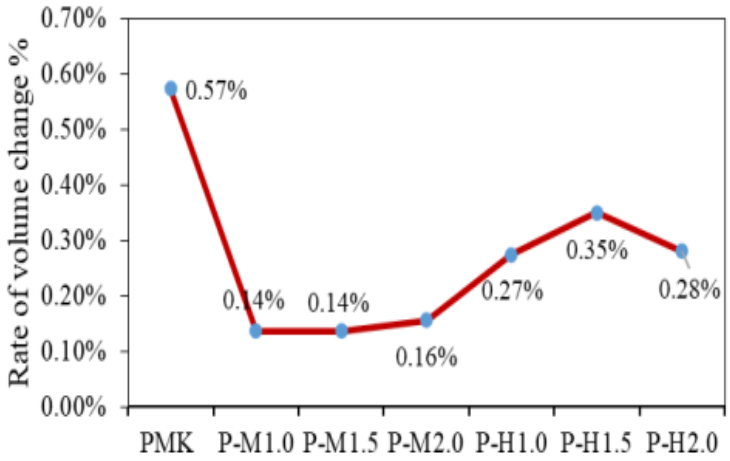

Figure 18 Volume Change Rate after 300 Hours of Dry-heat Aging

evidence for surface responses related to flexural strength degradation.

3.3.3 Volume Change Rate

The volume change rate after 300 hours of dry-heat aging at 70°C is shown in Figure 18, demonstrating the material's dimensional stability under dry-heat conditions. All specimens exhibited low volume change rates, ranging from 0.14% to 0.57%, indicating overall good dimensional stability. The neat paste (PMK) had the largest volume change rate at 0.57%, while the addition of aggregates significantly reduced this rate. The P-M system showed a volume change rate between 0.14%–0.16%, with minimal variation across different gradations, indicating a stable constraint effect from the mullite aggregates on volume shrinkage induced by dry-heat aging. The P-H system had a volume change rate ranging from 0.27% to 0.35%, which was higher than that of the P-M system but still lower than that of the neat paste, showing that the sandstone aggregates also helped mitigate macroscopic volume changes but were more sensitive to gradation and interface conditions.

Overall, the volume change rate followed the trend: PMK > P-H > P-M, with the P-M system exhibiting the best stability. This suggests that the introduction of aggregates, particularly mullite, plays a crucial role in improving the material's resistance to volume shrinkage under dry-heat conditions, with the P-M system showing the most consistent and stable behavior.

4. CONCLUSIONS

This study focused on the performance of restoration mortars based on the MK-MCPM phosphate gelling system, specifically designed for the Helankou rock art area. The mortars were prepared with different aggregates—mullite and Helankou sandstone—and evaluated under various weathering conditions, including freeze-thaw cycling, wet-dry cycling, and dry-heat aging.

The results indicate that the addition of aggregates significantly improved the mechanical properties, surface stability, and durability of the mortars compared to the neat paste. The P-M mortar, incorporating mullite aggregates, showed the best overall performance, with high strength retention, low mass loss, and minimal volume changes under extreme weathering conditions. The P-H mortar, made with Helankou sandstone aggregates, also demonstrated good durability, but its performance was more sensitive to gradation and interface quality, showing slightly higher strength losses and surface hardness degradation compared to the P-M system.

Under freeze-thaw and wet-dry cycling conditions, both mortars showed remarkable resistance to surface erosion and strength degradation, with the P-M mortar performing slightly better. The P-H mortar also exhibited satisfactory performance, although its flexural strength showed a greater degree of deterioration under wet-dry cycling. In dry-heat aging tests, the addition of aggregates significantly mitigated the strength and surface degradation typically seen in the neat paste, with the P-M system showing the best dry-heat stability.

Overall, the study demonstrates that the MK-MCPM repair mortars, especially those with mullite aggregates, have considerable potential for use in the restoration of rock art in the Helankou area. The performance

of these materials under harsh environmental conditions highlights their durability and suitability for long-term application. Future work should focus on optimizing the interface between aggregates and the matrix, as well as fine-tuning the gradation to further improve the long-term reliability of these restoration materials.

ACKNOWLEDGEMENT

This work was supported by the Ningxia Hui Autonomous Region Bureau of Cultural Relics under the project "Preliminary Survey and Research on the Protection of Helan Mountain Rock Paintings" (grant number: Ningwenwufa No. 83) and the China Postdoctoral Science Foundation (grant number: 2025M771677). We also thank the Yinchuan Municipal Administration of Helan Mountain Rock Art, 199 East Square Road, Yinchuan, Ningxia, China, for their assistance during field investigations.

REFERENCES

Arizzi, A., Martínez Martínez, J., Cultrone, G. (2011). Mechanical evolution of lime mortars during the carbonation process. *Key Engineering Materials*, *465*, 483–486. https://doi.org/10.4028/www.scientific.net/KEM.465.483

Bisschop, J., & van Mier, J. G. M. (2002). Effect of aggregates on drying shrinkage microcracking in cement-based composites. *Materials and Structures*, *35*(8), 453–461. https://doi.org/10.1007/BF02483132

Bui, H., Levacher, D., Boutouil, M., & Sebaibi, N. (2022). Effects of wetting and drying cycles on microstructure change and mechanical properties of coconut fibre-reinforced mortar. *Journal of Composite Science*, *6*(4), 102. https://doi.org/10.3390/jcs6040102

Chen, Q., Zhang, J., Wang, Z., & Zhao, T. (2024). A review of the interfacial transition zones in concrete: Identification, physical characteristics and mechanical properties. *Engineering Fracture Mechanics*, *300*, 109979. https://doi.org/10.1016/j.engfracmech.2024.109979

Dehestani, A., Hosseini, M., & Taleb Beydokhti, A. (2020). Effect of wetting-drying cycles on mode I and mode II fracture toughness of cement mortar and concrete. *Theoretical and Applied Fracture Mechanics*, *106*, 102448. https://doi.org/10.1016/j.tafmec.2019.102448

Deng, H., Zhou, S., Yu, S., Liu, Y., & Xu, J. (2025). Evolution of pore structure and mechanical characteristics of red sandstone under drying-wetting cycles. *Minerals*, *15*(2), 158. https://doi.org/10.3390/min15020158

Deprez, M., De Kock, T., De Schutter, G., & Cnudde, V. (2020). A review on freeze-thaw action and weathering of rocks. *Earth-Science Reviews*, *203*, 103143. https://doi.org/10.1016/j.earscirev.2020.103143

Feng, H., Wang, L., Yu, Z., Guo, A., & Liang, J. (2024). Freeze-thaw resistance and service life prediction of fly ash incorporated ultra-high ductility magnesium phosphate cement-based composites. *Construction and Building Materials*, *449*, 138330. https://doi.org/10.1016/j.conbuildmat.2024.138330

Hong, M., Lei, D., Zhu, F., Bai, P., & He, J. (2023). Experimental research on aggregate restrained shrinkage and cracking of early-age cement paste. *Cement and Concrete Research*, *172*, 107246. https://doi.org/10.1016/j.cemconres.2023.107246

Hu, W., Li, K., Yin, W., Zhang, H., Xue, Y., Han, Y., & Liu, P. (2024). Effects of wetting-drying cycles on the macro and micro properties of the cement-stabilized soil with curing agent. *Buildings*, *14*(6), 1716. https://doi.org/10.3390/buildings14061716

Huo, X., Ma, R., Xiong, Y., Ma, E., & Wang, J. (2024). Weathering disease characteristics and impact assessment of Helankou rock art. *Journal of Rock Art*, *3*(1), 09–19. https://doi.org/10.7508/jra.01.2024.09.19

Huo, X., Wang, J., Jiang, S., Li, J., Ma, E., & Wang, J. (2025). Assessing weathering damage to Helankou rock art by integrating morphological and in-situ performance data. *Journal of Rock Art*, *4*(2), 1–10. https://doi.org/10.65098/jra.02.2025.01.10

Jiang, S., Wang, J., Chen, J., Huo, X., & Cao, Y. (2025). A novel chemically bonded phosphate ceramics derived from metakaolin and monocalcium phosphate monohydrate for restoration of stone relics. *Applied Clay Science*, *275*, 107880. https://doi.org/10.1016/j.clay.2025.107880

Lubelli, B., Nijland, T. G., & van Hees, R. P. J. (2012). Simulation of the self-healing of dolomitic lime mortar. *Materiali in Tehnologije*, *46*(3), 291–296.

Maruyama, I., Kobayashi, T., & Nakajima, T. (2018). Effect of aggregate size on restrained shrinkage of concrete and mortar. *MOJ Civil Engineering*, *4*(1), 15–21. https://doi.org/10.15406/mojce.2018.04.00092

Powers, T. C. (1975). Freezing effects in concrete. *ACI Special Publication SP-47-1*. American Concrete Institute.

Rempel, A. W. (2007). Formation of ice lenses and frost heave. *Journal of Geophysical Research*, *112*, F02S21. https://doi.org/10.1029/2006JF000525

Song, Y., Wu, Q., Agostini, F., Skoczylas, F., & Bourbon, X. (2021). Concrete shrinkage and creep under drying/wetting cycles. *Cement and Concrete Research*, *140*, 106308. https://doi.org/10.1016/j.cemconres.2020.106308

Xu, B., Winnefeld, F., & Lothenbach, B. (2021). Effect of temperature curing on properties and hydration of wollastonite blended magnesium potassium phosphate cements. *Cement and Concrete Research*, *142*, 106370. https://doi.org/10.1016/j.cemconres.2021.106370

Yang, B., Ji, R. J., Lan, Q., Yang, J. M., & Xu, J. (2022). Sulfate freeze-thaw resistance of magnesium potassium phosphate cement mortar. *Materials*, *15*(9), 3342. https://doi.org/10.3390/ma15093342

Yuanquan, Y., Guanhua, Z., Jinbo, G., Dingwen, Q., & Runqing, L. (2023). An insight into the thermal properties of struvite-k by Rietveld refinement method. *Journal of Materials Research and Technology*, *24*, 2463–2474. https://doi.org/10.1016/j.jmrt.2023.04.032